Geophysical Research Letters

RESEARCH LETTER
10.1029/2023GL105401

Toward Understanding Polar Heat Transport Enhancement in Subglacial Oceans on Icy Moons

Robert Hartmann[1], **Richard J. A. M. Stevens**[1], **Detlef Lohse**[1,2], **and Roberto Verzicco**[1,3,4]

[1]Physics of Fluids Group and Max Planck Center for Complex Fluid Dynamics, J.M. Burgers Center for Fluid Dynamics, University of Twente, Enschede, The Netherlands, [2]Max Planck Institute for Dynamics and Self-Organisation, Göttingen, Germany, [3]Dipartimento di Ingegneria Industriale, University of Rome 'Tor Vergata', Rome, Italy, [4]Gran Sasso Science Institute, L'Aquila, Italy

Key Points:

- The polar heat transport in spherical rotating Rayleigh-Bénard convection experiences an enhancement by rotation
- The influence of rotation differs at low latitudes: the heat flux is reduced and compensates the polar enhancement on the global average
- In combination, this strengthens the latitudinal variation between polar and equatorial heat flux for Prandtl numbers larger than unity

Supporting Information:

Supporting Information may be found in the online version of this article.

Correspondence to:

R. Hartmann and R. Verzicco,
r.hartmann@utwente.nl;
verzicco@uniroma2.it

Citation:

Hartmann, R., Stevens, R. J. A. M., Lohse, D., & Verzicco, R. (2024). Toward understanding polar heat transport enhancement in subglacial oceans on icy moons. *Geophysical Research Letters*, *51*, e2023GL105401. https://doi.org/10.1029/2023GL105401

Received 19 JULY 2023
Accepted 22 JAN 2024

Author Contributions:

Conceptualization: Robert Hartmann, Richard J. A. M. Stevens, Roberto Verzicco
Data curation: Robert Hartmann, Richard J. A. M. Stevens
Formal analysis: Robert Hartmann
Funding acquisition: Richard J. A. M. Stevens
Investigation: Robert Hartmann
Methodology: Robert Hartmann, Roberto Verzicco
Project administration: Richard J. A. M. Stevens, Detlef Lohse, Roberto Verzicco

Abstract The interior oceans of several icy moons are considered as affected by rotation. Observations suggest a larger heat transport around the poles than at the equator. Rotating Rayleigh-Bénard convection (RRBC) in planar configuration can show an enhanced heat transport compared to the non-rotating case within this "rotation-affected" regime. We investigate the potential for such a (polar) heat transport enhancement in these subglacial oceans by direct numerical simulations of RRBC in spherical geometry for $Ra = 10^6$ and $0.7 \leq Pr \leq 4.38$. We find an enhancement up to 28% in the "polar tangent cylinder," which is globally compensated by a reduced heat transport at low latitudes. As a result, the polar heat transport can exceed the equatorial by up to 50%. The enhancement is mostly insensitive to different radial gravity profiles, but decreases for thinner shells. In general, polar heat transport and its enhancement in spherical RRBC follow the same principles as in planar RRBC.

Plain Language Summary The icy moons of Jupiter and Saturn like for example, Europa, Titan, or Enceladus are believed to have a water ocean beneath their ice crust. Several of them show phenomena in their polar regions like active geysers or a thinner crust than at the equator, all of which might be related to a larger heat transport around the poles from the underlying ocean. We simulate the flow dynamics and currents in these subglacial ocean by high-fidelity simulations, though still at less extreme parameters than in reality, to study the heat transport and provide a possible explanation of such a "polar heat transport enhancement." We find that the heat transport around the poles can be up to 50% larger than around the equator, and that the believed properties of the icy moons and their oceans would allow polar heat transport enhancement. Therefore, our results may help to improve the understanding of ocean currents and latitudinal variations in the oceanic heat transport and crustal thickness on icy moons.

1. Introduction

In the common understanding, most icy satellites in the solar system, for example, the Jovian and Saturnian moons Europa, Ganymede, Titan, and Enceladus, contain a global ocean layer beneath their ice crust (e.g., Nimmo & Pappalardo, 2016), which gained a lot of interest in terms of habitable environments (e.g., Chyba & Hand, 2005; Vance et al., 2018). In order to assess their habitability, it is crucial to understand their flow dynamics. On Enceladus, for instance, eruptions from fault systems at the south pole (see, e.g., Nimmo & Pappalardo, 2016) suggest a strong polar anomaly of enhanced heat transport. Furthermore, the crustal thickness counterintuitively decreases from the equator toward the poles (e.g., Beuthe et al., 2016; Čadek et al., 2019; Hemingway & Mittal, 2019; Kang, 2022; Kang & Jansen, 2022), which suggests a large-scale latitudinal variation of the heat released from the subglacial ocean (Kihoulou et al., 2023). In this study, we investigate possible dynamics inside and the heat transport out of such oceans by direct numerical simulations (DNSs) of rotating Rayleigh-Bénard convection (RRBC) in spherical geometry covering the full range from zero to rapid, nearly subcritical rotation. Therewith, we aim to elucidate a possible factor for a polar enhancement of the heat transport on icy moons.

The canonical RRBC system in planar configuration has been extensively studied experimentally and numerically (see, e.g., the reviews by Ecke & Shishkina, 2023; Kunnen, 2021; Plumley & Julien, 2019; Stevens et al., 2013, and Refs. therein). Its dynamical behavior is fully controlled by three dimensionless parameters: the Prandtl number Pr describing the fluid properties, the Rayleigh number Ra setting the strength of thermal driving, and the inverse Rossby number Ro^{-1} as a measure for the importance of rotation relative to buoyancy (full definitions in

Resources: Robert Hartmann, Richard J. A. M. Stevens, Detlef Lohse, Roberto Verzicco
Software: Robert Hartmann, Roberto Verzicco
Supervision: Richard J. A. M. Stevens, Detlef Lohse, Roberto Verzicco
Visualization: Robert Hartmann
Writing – original draft: Robert Hartmann
Writing – review & editing: Richard J. A. M. Stevens, Detlef Lohse, Roberto Verzicco

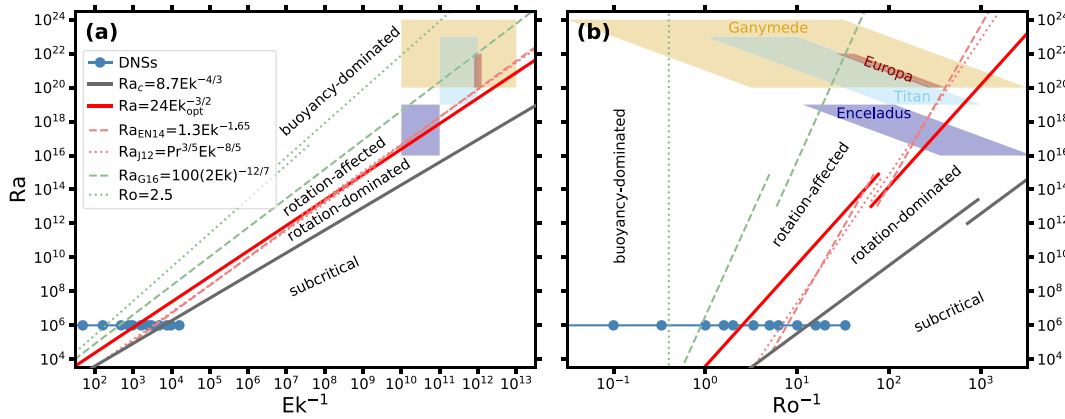

Figure 1. Regime diagram of (planar) rotating Rayleigh-Bénard convection (RRBC) in the parameter space of (a) Ra and Ek^{-1} and (b) Ra and Ro^{-1} (after Soderlund (2019), see also Kunnen (2021)): The solid gray line denotes the critical Rayleigh number Ra_c for the onset of convection (Chandrasekhar, 1961). The solid red line depicts the transition between the rotation-dominated and the rotation-affected regimes based on boundary layer crossing and heat transport maximum per fixed Ra for $Pr > 1$ fluids (Yang et al., 2020). Dashed and dotted light red lines are alternative estimates for this transition by Ecke and Niemela (2014) and Julien, Knobloch, et al. (2012), respectively. The dashed and dotted green lines represent the transition between the rotation-affected and the buoyancy-dominated regimes based on Gastine et al. (2016) and for a cylinder with diameter-to-height ratio 1 (Weiss et al., 2010), respectively. The blue circles mark the simulations of spherical RRBC in this study ($Pr = 4.38$). The shaded areas show the predicted parameter range for several icy moons ($10 \leq Pr \leq 13$) as given in Soderlund (2019). Line offsets symbolize the Pr dependence of any transition between $Pr = 4.38$ like in our simulations and $Pr = 13$ like the upper bound for the icy moons.

Section 2). The influence of rotation can alternatively be parameterized by the Ekman number $Ek = Ro\sqrt{Pr/Ra}$. Several flow regimes and flow states were discovered and studied over the past decades. The three major regimes based on the trend of heat transport with varying rotation are (a) the *buoyancy-dominated* regime at relatively slow rotation, where heat transport and flow dynamics remain unaffected compared to the non-rotating case, (b) the transitional *rotation-affected* regime, where intermediate rotation starts to alter the flow, and (c) the *rotation-dominated* regime for rapid rotation, where the heat transport steeply decreases with increasing rotation as it impedes vertical motion (Proudman, 1916; Taylor, 1917), see for example, Kunnen (2021) and Ecke and Shishkina (2023). Both rotation-affected and rotation-dominated regimes show a broad variety of subregimes or flow states, all of which are characterized by columnar vortical structures aligned with the rotation axis (e.g., Aguirre Guzmán et al., 2020; Cheng et al., 2015; Julien et al., 1996; Julien, Rubio, et al., 2012; Sprague et al., 2006; Stellmach et al., 2014; Stevens et al., 2009). Due to the huge variety of flow states, there exist various estimates for the boundaries of the above regimes in the literature (see Kunnen (2021) for a detailed overview)—most of them based on RRBC data in the planar configuration. The most common ones are summarized in Figure 1.

An important peculiarity of planar RRBC with $Pr > 1$ is that Ekman pumping through vertically coherent vortices enhances the heat transport in the rotation-affected regime to exceed its non-rotating value (e.g., Kunnen et al., 2006; Rossby, 1969; Stevens et al., 2013; Zhong et al., 2009). The enhancing effect is most efficient when thermal and kinetic boundary layers have approximately the same thickness (e.g., Julien et al., 2016; Stevens et al., 2010; Yang et al., 2020). This creates a heat transport maximum (per fixed Ra) that follows $Ra \propto Ek^{-3/2}$ (Figure 1, red line; King et al., 2012; Yang et al., 2020). For very turbulent flows when $Ra/Pr \gtrsim 10^8$ (Hartmann et al., 2023), the maximum diverges toward weaker rotation and the enhancement magnitude decreases (Yang et al., 2020).

Parameter estimates for icy moon ocean worlds still vary over a wide range (Bire et al., 2022; Soderlund, 2019). Based on the estimates by Soderlund (2019), the subglacial oceans of Europa, Ganymede, Titan, and Enceladus would be situated in the rotation-affected regime (see Figure 1). Given that the water of these oceans has $Pr \in [10, 13]$ (Soderlund, 2019), they arguably have the potential for heat transport enhancement—at least around the poles, where buoyancy is mostly aligned with the rotation axis as in planar RRBC. Such a polar heat transport enhancement could strengthen the latitudinal heat transport variations that are observed in spherical RRBC with $Pr = 1$ (e.g., Amit et al., 2020; Bire et al., 2022; Kvorka & Čadek, 2022; Soderlund, 2019). We therefore

distinguish between two types of heat transport enhancement: (a) enhancement above the non-rotating heat transport in a specific region is considered as, for example, *polar*, *equatorial*, or *global enhancement*, whereas (b) a larger heat transport at the poles than at the equator is referred to as *latitudinal enhancement*. Since most simulations of spherical RRBC are conducted for $Pr = 1$ (e.g., Gastine et al., 2016; Soderlund et al., 2012; Wang et al., 2021) and all studies on rotation-induced heat transport enhancement focus on planar RRBC (e.g., Stevens et al., 2009, 2010; Weiss et al., 2016; Yang et al., 2020), we aim to bridge this gap and elucidate the potential of spherical RRBC to show polar and/or global heat transport enhancement. Therefore, we set $Pr = 4.38$ as in many simulations and experiments of planar RRBC and cover the entire range of regimes (Figure 1).

In the following, we introduce spherical RRBC, its control parameters, and our numerical method (Section 2). Then, latitudinal variations of the heat transport are analyzed and linked to the predominant structures in the flow (Secton 3). Subsequently, we discuss the importance of $Pr > 1$ by a direct comparison with $Pr \leq 1$ (Section 4), the influence of the shell thickness, representing the ocean depth (Section 5), the sensitivity to different radial gravity profiles (Section 6), and the relevance of the ratio between thermal and kinetic boundary layers for heat transport enhancement in spherical RRBC (Section 7). The letter ends with conclusions (Section 8).

2. Dynamical Equations and Numerical Method

Spherical RRBC describes the dynamics of a fluid in a spherical shell confined by a hot inner and a cold outer sphere, rotating around a polar axis (Figure 2b) (e.g., Aurnou et al., 2015; Busse, 1970, 1983; Roberts, 1968). The geometry of the system is determined by the inner and outer radii r_i and r_o, defining the shell thickness $H = r_o - r_i$ expressed by the radius ratio $\eta = r_i/r_o$. The dynamics are controlled by the three dimensionless parameters Pr, Ra, and Ro^{-1}, defined as:

$$Pr = \frac{\nu}{\kappa},\ Ra = \frac{\alpha g_0 \Delta T H^3}{\nu\kappa},\ Ro^{-1} = \frac{2\Omega H}{\sqrt{\alpha g_0 \Delta T H}}. \tag{1}$$

Therein, ν is the kinematic viscosity, κ the thermal diffusivity, α the isobaric thermal expansion coefficient, g_0 the reference gravitational acceleration at the outer sphere, ΔT the temperature difference between inner and outer sphere, and Ω the angular rotation rate, respectively. Under Oberbeck-Boussinesq approximation, the system is governed by the continuity, Navier-Stokes and temperature convection-diffusion equations, which are given in dimensionless form as:

$$\nabla \cdot \vec{u} = 0, \tag{2}$$

$$\frac{\mathrm{d}\vec{u}}{\mathrm{d}t} = -\nabla P + \sqrt{\frac{Pr}{Ra}}\nabla^2\vec{u} + \Theta\frac{g(r)}{g_0}\vec{e}_r - \frac{1}{Ro}\vec{e}_z \times \vec{u}, \tag{3}$$

$$\frac{\mathrm{d}\Theta}{\mathrm{d}t} = \frac{1}{\sqrt{Pr\ Ra}}\nabla^2\Theta. \tag{4}$$

Therein, $\vec{u}$, P, and Θ denote the normalized velocity, pressure, and temperature fields, respectively. $\mathrm{d}/\mathrm{d}t$ denotes the full, so-called material derivative. $g(r) = g_0\,(r/r_o)^\gamma$ accounts for radial variations in the gravity profile. The equations are normalized by H and the free-fall velocity $U_0 = \sqrt{\alpha g_0 \Delta T H}$. The temperature is normalized as $\Theta = \frac{T - T_{\mathrm{top}}}{\Delta T} \in [0, 1]$. The pressure field P is reduced by the hydrostatic balance and centrifugal contributions. We consider Coriolis forcing from constant rotation around the polar axis, but neglect centrifugal contributions on buoyancy. Isothermal and no-slip boundary conditions are imposed at the hot inner ($\Theta = 1$) and the cold outer ($\Theta = 0$) spheres.

In this study, we conduct DNSs of spherical RRBC at $Ra = 10^6$ with $Pr = 4.38$, 1 and 0.7 in the range of $0 \leq Ro^{-1} \leq 33.\bar{3}$ ($0 \leq Ek^{-1} \lesssim 1.6 \cdot 10^4$) for different radius ratios η and gravity profiles $g(r)$. For the chosen parameters, the Reynolds numbers expectably remain relatively low ($\mathrm{Re} \lesssim 270$, see Tables S1–S3 in Supporting Information S1). The DNSs solve the governing equations (Equations 2–4) by a central second-order accurate finite-difference scheme based on a staggered grid discretization in spherical coordinates (Santelli et al., 2020), which has been rigorously validated in subsequent studies (Wang et al., 2021, 2022). The computational grid is

uniformly spaced in the longitudinal and latitudinal directions, while the grid points in the radial direction are clustered toward the inner and outer spheres. This ensures an appropriate resolution of the Kolmogorov scales in the bulk, as well as of the boundary layers (Shishkina et al., 2010). A summary of grid sizes and numerical parameters can be found in Text S1, Tables S1–S3 of Supporting Information S1.

3. Polar Heat Transport Enhancement

We begin our investigation on a rather thick shell of $\eta = 0.6$ with constant gravity $g(r) = g_0$. The dimensionless heat transport is given by the Nusselt number Nu. We first consider Nu on the outer sphere as a function of the latitude φ:

$$Nu_{r_o}(|\varphi|) = -\frac{1}{\eta}\partial_r \langle \Theta \rangle_{t,\vartheta,\pm\varphi}\big|_{r_o}. \tag{5}$$

Therein $\langle\cdot\rangle_{t,\vartheta,\pm\varphi}$ indicates averaging in time, longitude, and latitudinal symmetry around the equator. For no and slow rotation ($Ro^{-1} \leq 0.3$), the heat transport is expectably uniform over φ (Figure 2a). Accordingly, the flow is dominated by radial buoyant plumes (Figure 2c), which can organize in a persistent large-scale circulation pattern. Such large-scale circulations are well known from other non-rotating geometries, for example, RBC in cylindrical containers (e.g., Ahlers et al., 2009, and Refs. therein), 2D RBC (e.g., van der Poel et al., 2013, and Refs. therein), or extremely wide domains (Stevens et al., 2018). However, without rotation, the heat transport ideally is radially symmetric, defining a reference value $Nu_0 = \langle Nu_{r_o}\rangle_\varphi\left(Ro^{-1} = 0\right)$ (Figure 2a, horizontal dashed line).

At intermediate rotation rates ($1 \leq Ro^{-1} \leq 5$), the heat transport is reduced toward the equator and enhanced toward the poles compared to the non-rotating reference (Figure 2a). Taylor columns aligned with the rotation axis form in the flow (Figure 2d) and alter the heat transport. Their vortical motion impedes the radial heat transport around the equator and leads to the formation of sheet-like thermal plumes around the columnar structures (similar to Aurnou et al., 2015; Soderlund et al., 2012). On the contrary, the Taylor columns support the radial heat transport around the poles by Ekman pumping through their interior (in presence of no-slip boundary conditions, e.g., Stellmach et al. (2014)). For $\eta = 0.6$, the polar tangent cylinder, that is, the cylinder around the inner sphere aligned with the polar axis, intersects with the outer sphere at latitude $|\varphi_{tc}| = 53.13°$. We use $|\varphi_{tc}|$ to distinguish between the "polar region" ($|\varphi_{tc}| < |\varphi| < 90°$), in which ideal axial Taylor columns connect the hot inner sphere with cold outer sphere, and the "low-latitude region" ($|\varphi_{tc}| > |\varphi| > 0°$), in which axial Taylor columns connect the Northern and Southern hemispheres of the outer sphere (Figure 2b). For $1 \leq Ro^{-1} \leq 5$, $|\varphi_{tc}|$ clearly correlates with the transition from reduced to enhanced heat transport $\left(Nu_{r_o}\left(|\varphi_{tc}|\right) \approx Nu_0\right)$. The rather smooth trend of $Nu_{r_o}(|\varphi|)$ across $|\varphi_{tc}|$ however suggests that the inclination between buoyancy (radial) and rotation (axial) additionally influences the enhancement with latitude (as similarly argued by Gastine & Aurnou, 2023).

For rapid rotation ($Ro^{-1} \geq 10$), the latitudinal trend in the heat transport is inverted (Figure 2a). At high latitudes, the heat transport quickly decreases with increasing Ro^{-1} down to $Nu_{r_o} = 1$. Toward the equator, the heat transport first increases slightly (compared to the reduction at intermediate rotation), before it also decreases with increasing Ro^{-1}. With increasing rotation the fluid motion is suppressed in the axial direction and becomes strongly focused in the orthogonal planes (Proudman, 1916; Taylor, 1917, 1923). Thus, convection halts inside the tangent cylinder and the radial heat transport mostly aligned with the rotation axis becomes purely conductive. Toward the equator, quasi-2D vortical motion aligns with radial buoyancy, which helps to longer sustain convective heat transport via sheet-like plumes (Figure 2e). Also for rapid rotation, $|\varphi_{tc}|$ depicts a major transition in the trend of $Nu_{r_o}(|\varphi|)$, namely where the heat transport starts to increase toward its equatorial peak value (Figure 2a, see also Gastine & Aurnou, 2023; Wang et al., 2021).

Overall, Figure 2 shows that heat transport enhancement, as known from planar RRBC, is limited to high latitudes inside the tangent cylinder in spherical RRBC. In order to further quantify the polar enhancement, we consider the radial heat transport at the outer sphere averaged (a) over the polar region $Nu_{tc} = \langle Nu_{r_o}\rangle_{|\varphi|>|\varphi_{tc}|}$, (b) in the complementary low-latitude region $Nu_{ll} = \langle Nu_{r_o}\rangle_{|\varphi|<|\varphi_{tc}|}$, and (c) globally over the entire sphere $\langle Nu_{r_o}\rangle_\varphi$. In this way, we can demonstrate that the heat transport in the polar region Nu_{tc} shows the typical enhancement behavior of planar RRBC (Figure 3a, red triangles). Together with the results above (Figure 2), it becomes clear that the

10.1029/2023GL105401

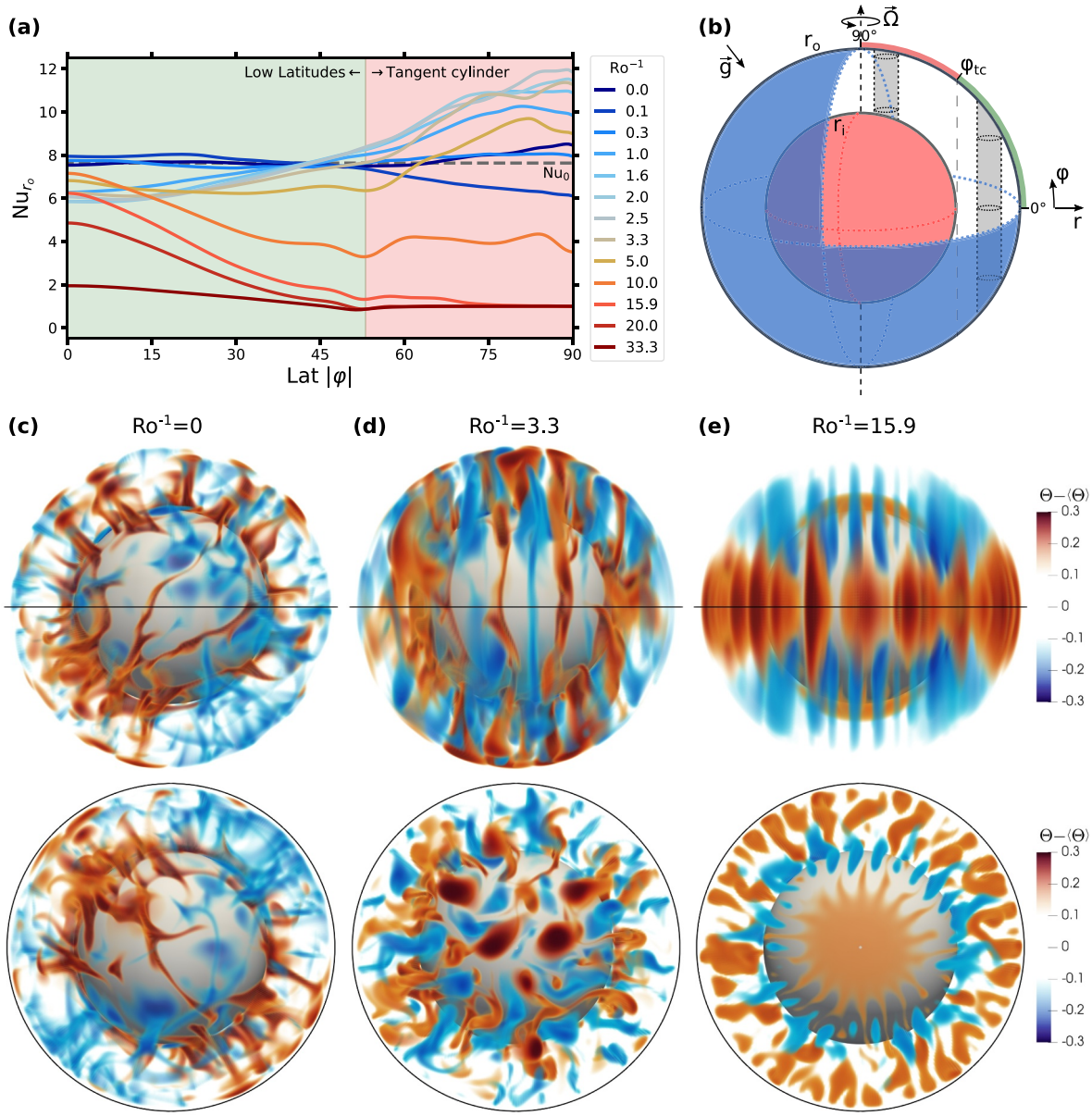

Figure 2. (a) Dimensionless heat transport at the outer sphere Nu_{r_o} as function of the latitude $|\varphi|$ for various rotation rates Ro^{-1} at $Ra = 10^6$ and $Pr = 4.38$ with $\eta = 0.6$ and constant $g(r) = g_0$. (b) Schematic view on spherical rotating Rayleigh-Bénard convection showing the idealized arrangement of axially aligned Taylor columns inside and outside the polar tangent cylinder. (c–e) Corresponding 3D snapshots of the temperature fluctuations $\Theta' = \Theta - \langle\Theta\rangle_{\vartheta,\varphi}$ at no rotation ($Ro^{-1} = 0$), intermediate rotation $\left(Ro^{-1} = 3.\bar{3}\right)$, and rapid rotation ($Ro^{-1} = 15.9$), respectively, viewed from the equator (top) and the South pole (bottom).

basic mechanisms, which cause the polar enhancement, remain the same, namely: the formation of axially coherent vortical structures bridging the bulk between the hot and the cold source such that Ekman pumping of relatively hot/cold fluid from the boundary layers can support the heat transport along the axial direction. However, no enhancement is found for the global heat transport of the full Rayleigh-Bénard sphere (Figure 3a, gray circles). The enhanced heat transport inside the polar region is globally balanced by the reduced heat transport in the low-latitude region (Figure 3a, green squares). It seems that the equatorial reduction strengthens as the polar enhancement increases.

The amplitude of polar heat transport enhancement compared to Nu_0 reaches ≈28% (Figure 3a, red triangles), which is comparable with the enhancement observed in planar RRBC (e.g., Kunnen et al., 2011; Yang et al., 2020;

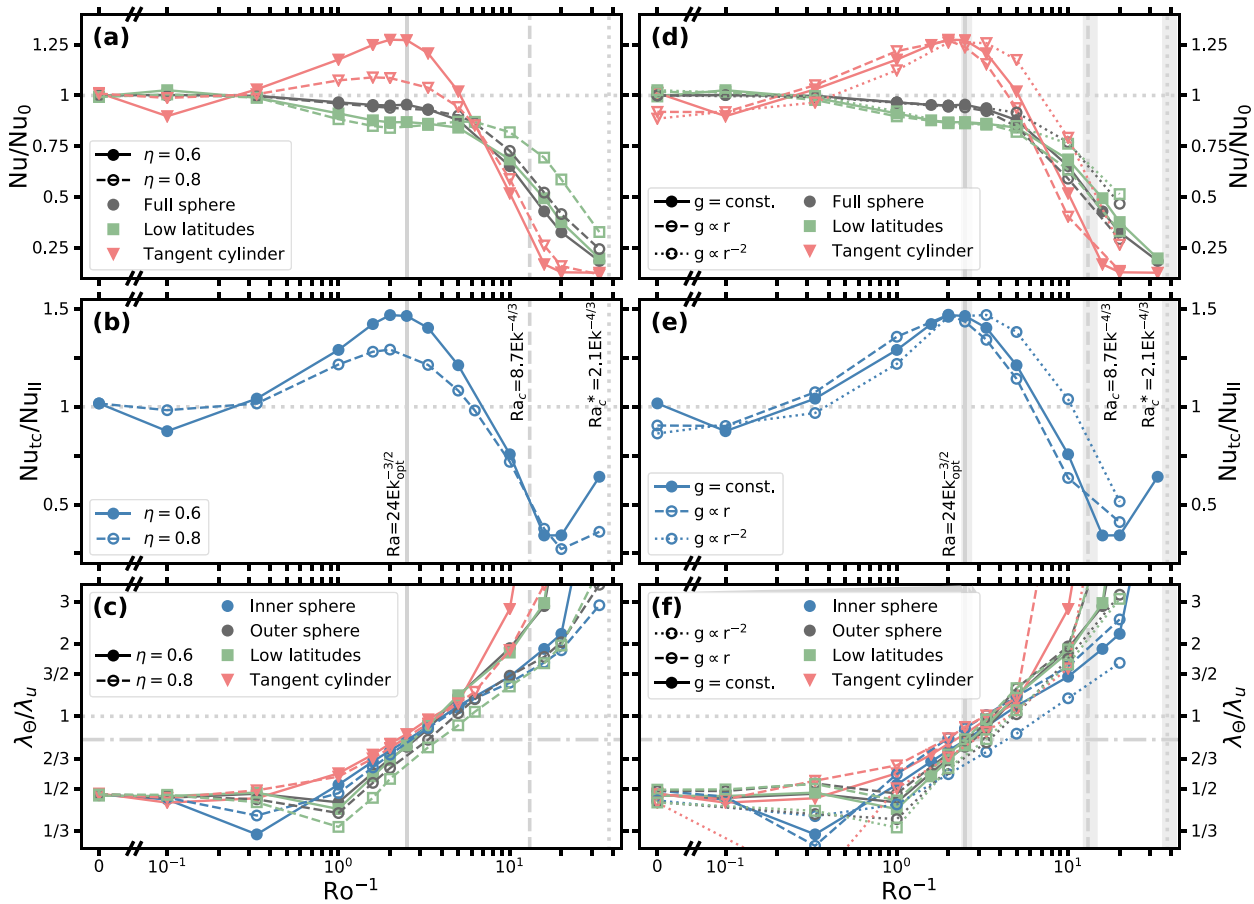

Figure 3. (a, d) Heat transport Nu relative to the non-rotating reference Nu_0 as a function of Ro^{-1} for the full sphere $\left(Nu \equiv \langle Nu_{r_o} \rangle_\varphi\right)$, in the polar region $\left(Nu_{\mathrm{tc}} = \langle Nu_{r_o} \rangle_{|\varphi| > |\varphi_{\mathrm{tc}}|}\right)$, and in the complementary low-latitude region $\left(Nu_{\mathrm{ll}} = \langle Nu_{r_o} \rangle_{|\varphi| < |\varphi_{\mathrm{tc}}|}\right)$. (b, e) Ratio between the heat transport in the polar region Nu_{tc} and the low-latitude region Nu_{ll} as a function of Ro^{-1}. (c, f) Ratio of thermal and kinetic boundary layer thicknesses λ_Θ/λ_u as a function of Ro^{-1} averaged over the inner sphere, the outer sphere, the polar region, and the low-latitude region. (left) For different η with constant $g(r) = g_0$, and (right) for different $g(r) \propto r^\gamma$ with fixed $\eta = 0.6$. All data at $Pr = 4.38$, $Ra = 10^6$. The solid, dashed, and dotted vertical lines mark the predicted optimal rotation rate Ro_{opt}^{-1} in planar rotating Rayleigh-Bénard convection (RRBC) given by $Ra = 24Ek^{-3/2}$ (King et al., 2012; Yang et al., 2020), and the predicted onsets of convection in planar and spherical RRBC given by $Ra_c = 8.7Ek^{-4/3}$ (Chandrasekhar, 1961) and $Ra_c^*(\eta = 0.6) \approx 2.1Ek^{-4/3}$ (estimated from Barik et al., 2023), respectively. The influence of Ra_{eff} on these transitions (shaded areas) are very limited (see Sections 6 and 7). The dotted and dashed-dotted horizontal lines emphasize ratio 1 and 0.8, respectively.

Zhong et al., 2009). The polar enhancement is even larger when only a narrower region directly around the poles is considered (see Figure S1 in Supporting Information S1), which emphasizes the additional influence of the tilt between buoyancy and rotation. Despite the absence of a global heat transport enhancement (relative to Nu_0 of the non-rotating system), the spatial large-scale variations of the heat transport are more important in geo- and astrophysical contexts, like the ocean dynamics of the icy moons. A direct comparison of $Nu_{\mathrm{tc}}/Nu_{\mathrm{ll}}$ yields up to ≈50% larger heat transport in the polar region than in the low-latitude region at the maximal polar enhancement (Figure 3b, full circles). For strong rotation this ratio inverts as convection halts earlier in the tangent cylinder and will again saturate at 1 once the system is fully in rest (Gastine & Aurnou, 2023).

4. Dependence on the Prandtl Number

Heat transport enhancement relative to Nu_0 in planar RRBC essentially depends on Pr. No clear enhancement due to rotation is observed for $Pr < 1$ as the thermal boundary layer is always thinner than the kinetic Ekman layer (King & Aurnou, 2013; Stevens et al., 2010; Yang et al., 2020). To validate this Pr dependence, we conducted additional series of DNSs for $Pr = 1$ and 0.7 (see Table S3 in Supporting Information S1). As expected, the heat transport enhancement Nu/Nu_0 inside the polar tangent cylinder of spherical RRBC vanishes (see Figure S2a in

Supporting Information S1). Interestingly, the heat transport in the low-latitude region also decreases with smaller Pr. Therefore, we can still observe some latitudinal enhancement $Nu_{\mathrm{tc}}/Nu_{\mathrm{ll}} > 1$ for $Pr = 0.7$ (see Figure S2b in Supporting Information S1) without any polar enhancement $Nu/Nu_0 < 1$. This agrees with the results from Soderlund (2019) performed at $Pr = 1$. However, the latitudinal enhancement $Nu_{\mathrm{tc}}/Nu_{\mathrm{ll}}$ is significantly smaller than for $Pr = 4.38$. Based on this trend, we conclude that, the polar enhancement Nu/Nu_0, which typically intensifies with increasing Pr above unity, will additionally amplify the latitudinal enhancement $Nu_{\mathrm{tc}}/Nu_{\mathrm{ll}}$. Since Pr also affects the heat transport in the low-latitude region, we speculate that for $Pr \gg 1$, even an enhancement of the global heat transport Nu/Nu_0 is possible. We note that these observations are opposite to the Pr trends observed with free-slip boundaries (Kvorka & Čadek, 2022).

5. Influence of Shell Thickness

In fact, the oceans of icy satellites are much thinner water layers, hence characterized by a much larger radius ratio than the previous $\eta = 0.6$. For the popular icy satellites indicated in Figure 1, the estimates are in a range of $0.74 < \eta < 0.99$ (Soderlund, 2019; Vance et al., 2018). A larger η also results in a larger polar tangent cylinder, in which the axial columns connect inner and outer sphere. When we increase the radius ratio to $\eta = 0.8$, the tangent cylinder starts already at $\varphi_{\mathrm{tc}} \approx 36.87°$ (compared to $\varphi_{\mathrm{tc}} \approx 53.13°$ for $\eta = 0.6$). Interestingly, the heat transport enhancement in the polar tangent cylinder drops to only ≈9%, whereas the full sphere average remains unchanged throughout the rotation-affected regime (Figure 3a, open symbols). This confirms the trend observed in Bire et al. (2022). Still, it seems counterintuitive since one would rather expect a constant enhancement amplitude in the enlarged tangent cylinder, which also affects the global heat transport. We speculate that the increasing inclination between radial buoyancy and axial rotation toward the edge of wider tangent cylinders reduces the efficiency of vortices pumping heat in the axial direction. Further, the heat transport enhancement directly around the poles reduces from $Nu_{\mathrm{pl}}/Nu_0 \approx 1.47$ for $\eta = 0.6$ to $Nu_{\mathrm{pl}}/Nu_0 \approx 1.26$ for $\eta = 0.8$ (see Figures S1 and S3 in Supporting Information S1), presumably saturating at such a planar-like enhancement amplitude for even larger η. Regardless, the heat transport inside the tangent cylinder can still be significantly larger than at the equator, resulting in a latitudinal enhancement up to ≈25% for $\eta = 0.8$ (Figure 3b, open symbols). The optimal rotation rate Ro_{opt}^{-1}, at which the maximal enhancements are achieved, remains mostly unaffected.

In the rotation-dominated regime, the heat transport in the polar region decreases similarly with Ro^{-1} for both η. Convection in the tangent cylinder ceases around $Ro_c^{-1} = 8.7^{-3/4} Pr^{1/2} Ra^{1/4} \approx 13.06$ (Figure 3a, vertical dashed line), derived from the predicted critical Rayleigh number $Ra_c = 8.7\ Ek^{-4/3}$ in planar RRBC (Chandrasekhar, 1961). On the contrary, faster rotation is necessary to suppress convective heat transport in the low-latitude region for larger η. This reflects that the critical Rayleigh number Ra_c^* for the equatorial onset of convection in spherical RRBC additionally depends on η, meaning $Ra_c^* = f(\eta, \ldots)\, Ek^{-4/3}$ (see Al-Shamali et al., 2004; Barik et al., 2023; Dormy et al., 2004), in contrast to Ra_c in planar RRBC valid in the likewise oriented tangent cylinder. We find a good agreement for the equatorial onset in our $\eta = 0.6$ data at $Ra_c^*(\eta = 0.6) \approx 2.1\, Ek^{-4/3}$ (see Figure 3, Figure S1 in Supporting Information S1), estimated from the results shown in Barik et al. (2023) for $\eta \approx 0.6$ and $Ek \approx 10^{-4}$ to 10^{-5}.

Lastly, we note the different slopes of the heat transport in the polar and the low-latitude region in the rotation-dominated regime. They can be attributed to "steep scaling" $Nu \propto \left(Ra\, Ek^{4/3}\right)^3 \propto Ro^4$ in the polar region where Ekman pumping plays an active role (Gastine & Aurnou, 2023; Julien et al., 2016; King et al., 2012, 2013; Plumley et al., 2016) and (the onset of) "diffusion-free scaling" $Nu \propto \left(Ra\, Ek^{4/3}\right)^{3/2} \propto Ro^2$ in the low-latitude region (Gastine et al., 2016; Wang et al., 2021). More detailed evidence for this can be found in Text S2 and Figure S4 of Supporting Information S1.

6. Sensitivity to Different Gravity Profiles

We further investigate the influence of different radial gravity profiles $g(r) = g_0\, (r/r_o)^\gamma$. Besides a constant gravity ($\gamma = 0$), we apply a homogeneous self-gravitating profile ($\gamma = 1$) and a mass-centered profile ($\gamma = -2$). For this, we stick to $\eta = 0.6$, because the radial gravity variation is larger in thicker shells and so is its potential impact on the heat transport. Aside from minor deviations, we cannot observe major differences in the normalized heat transport Nu/Nu_0 in the rotation-affected regime (until the polar heat transport maximum), including the amplitude of the polar and latitudinal enhancement maxima and their optimal rotation rate Ro_{opt}^{-1} (Figures 3d and

3e). One might spot a small shift in Ro^{-1} with γ. Its trend likely arises from a change of the effective Rayleigh number of the system $Ra_{\text{eff}} = \langle Ra(r)\rangle_r$, when the gravity varies with r: $Ra_{\text{eff}}(\gamma = 1) < Ra_{\text{eff}}(\gamma = 0) = Ra < Ra_{\text{eff}}(\gamma = -2)$ (see Text S3 in Supporting Information S1). Solely in the rotation-dominant regime (beyond the polar heat transport maximum), the heat transport remains considerably larger for smaller γ, hence increasing Ra_{eff}. Thus, the relative heat transport enhancement Nu/Nu_0 for $Ro^{-1} \leq Ro_{\text{opt}}^{-1}$ is mostly unaffected by the gravity profile $g(r) = r^{\gamma}$, in contrast to the absolute values Nu (Gastine et al., 2015; Wang et al., 2022). Especially the amplitude of the polar enhancement maximum Nu_{max}/Nu_0 seems to be insensitive to $g(r)$.

7. Relevance of the Boundary Layer Ratio

In planar RRBC, the heat transport maximum for $Ra/Pr \lesssim 10^8$ is typically associated with an equal thickness of the thermal and kinetic boundary layers λ_Θ and λ_u (Stevens et al., 2010), which theoretically scales as $\lambda_\Theta/\lambda_u \propto Ek^{3/2}Ra$ (King et al., 2012) giving an estimate for the optimal rotation rate at relatively low Ra (Yang et al., 2020):

$$Ro_{\text{opt}}^{-1} \approx 0.12\ Pr^{1/2}Ra^{1/6} \text{ or } Ra \approx 24\ Ek_{\text{opt}}^{-3/2}\ . \tag{6}$$

The predicted Ro_{opt}^{-1} nicely aligns with the heat transport maxima in the polar tangent cylinder independent of η and $g(r)$ (Figures 3a and 3d, solid vertical line). Taking Ra_{eff} into account yields $Ro_{\text{opt},\gamma=1}^{-1} \approx 0.97\, Ro_{\text{opt},\gamma=0}^{-1}$ and $Ro_{\text{opt},\gamma=-2}^{-1} \approx 1.07\, Ro_{\text{opt},\gamma=0}^{-1}$ (see Text S3 in Supporting Information S1). Both predicted and observed shifts of Ro_{opt}^{-1} with γ are mostly negligible.

We further verify the predicted boundary layer crossing by directly computing λ_Θ and λ_u from our DNSs as the height of the first peak in the radial profiles of the laterally averaged root-mean-square temperature and lateral velocity, respectively. Due to the asymmetry of cooling and heating in spherical RRBC, the boundary layer thicknesses differ between inner and outer sphere (Gastine et al., 2015). Therefore, we consider λ_Θ and λ_u separately averaged over (a) the inner and (b) the outer spheres. In addition to the spatial average over the full spheres, we again distinguish between (c) the polar and (d) the low-latitude regions on the outer sphere. Our data confirm such a typical boundary layer crossing for all the regions (a)–(d) in the spherical geometry—independent of η (Figure 3c). Furthermore, the polar heat transport maxima and the predicted Ro_{opt}^{-1} perfectly match to an observed boundary layer ratio of $\lambda_\Theta/\lambda_u \approx 0.8$ (dotted horizontal line), especially for the polar region (red symbols) and the inner sphere (blue symbols). This fully agrees with the observations of Yang et al. (2020) in planar RRBC based on the same boundary layer definitions. Only for the thinner $\eta = 0.8$ shell, the boundary layer ratio of the low-latitude region (and consequently also for the full outer sphere) lie slightly below the expected $\lambda_\Theta/\lambda_u \approx 0.8$. We also relate this to the different flow orientation at the equator, where the inner and outer shells act more like a sidewall for the axial vortex structures compared to the classical configuration in planar RRBC and the alike tangent cylinder. It therefore is even more remarkable that the boundary layer ratio also matches for the low-latitude region in the other cases. For variations of $g(r)$, the agreement with 0.8 is still very good (Figure 3f). These findings strengthen the argumentation by Amit et al. (2020) and Bire et al. (2022) that the transition between "polar and equatorial cooling" follows $Ra \propto Ek^{3/2}$.

8. Conclusions

Our DNSs of spherical RRBC with Pr larger than unity ($Pr = 4.38$) confirm the main features of heat transport enhancement, as known from planar RRBC, to similarly occur in the spherical geometry:

1. The three major regimes (buoyancy-dominated, rotation-affected, rotation-dominated) for the heat transport behavior of RRBC can be identified (Ecke & Shishkina, 2023; Kunnen, 2021).
2. *Intermediate* rotation enhances the heat transport up to ≈28% compared to the non-rotating case inside the polar tangent cylinder, where buoyancy is mostly aligned with the rotation axis and axially coherent vortices (Taylor columns) connect the hot inner with the cold outer shell.
3. The maximal (polar) enhancement is determined by an equal thickness of the thermal and kinetic boundary layers $\lambda_\Theta/\lambda_u \approx 1$. The associated optimal rotation rate $Ro_{\text{opt}}^{-1} \Leftrightarrow Ek_{\text{opt}}^{-1}$ can still be predicted via $Ra \approx 24\ Ek^{-3/2}$ as in planar RRBC (King et al., 2012; Yang et al., 2020).

We however find that the polar heat transport enhancement is accompanied by a reduced heat transport at low latitudes outside the tangent cylinder, where buoyancy is mostly orthogonal to the rotation axis and the axially coherent vortices can only connect both hemispheres of the cold outer shell. The equatorial reduction compensates the polar enhancement on the global average on the one hand, which on the other hand results in an even larger latitudinal enhancement of up to ≈50% between the polar and the low-latitude region.

We further clarified that the relative heat transport enhancements Nu/Nu_0 and Nu_{tc}/Nu_{ll} are mostly unaffected by the radial gravity profile. Rather surprisingly, a thinner shell ($\eta = 0.8$), which comes along with a larger tangent cylinder, shows less but still significant enhancement (≈9% for Nu/Nu_0 and ≈25% for Nu_{tc}/Nu_{ll}). While we expect the enhancement closely around the poles to converge for large η, the outer region of wide tangent cylinders will likely show less or no enhancement due to the inclination between rotation and buoyancy, urging for a better objective separation. This and the impression that the polar enhancement remains globally compensated by the equatorial reduction call for consecutive studies toward larger η, and for larger Pr.

The existence of polar heat transport enhancement in spherical RRBC, which increases the latitudinal difference between polar and equatorial heat transport, implies that accounting for $Pr > 1$ can be crucial for simulations of icy satellite oceans. Heat transport enhancement on the one hand increases with larger Pr (e.g., Stevens et al., 2010; Zhong et al., 2009) but on the other hand decreases with larger Ra (e.g., Yang et al., 2020). Hence, the question on how much enhancement persists on icy satellites with $Pr > 4.38$ ($10 \lesssim Pr \lesssim 13$) and $Ra \gg 10^6$ ($10^{16} \lesssim Ra \lesssim 10^{24}$) needs to be addressed differently as DNS cannot reach these parameters. Similarly, the effects of salinity (see e.g., Ashkenazy & Tziperman, 2021; Kang et al., 2022; Zeng & Jansen, 2021) on the enhancement needs to be further clarified. However, our findings show, in line with evidences from previous studies (Amit et al., 2020; Bire et al., 2022; Kvorka & Čadek, 2022; Soderlund, 2019), that in principle large-Pr related heat transport enhancement could serve as an explanation for latitudinal heat transport and associated ice thickness variations on icy satellites.

Data Availability Statement

The data on which this article is based are openly available in Hartmann (2023).

Acknowledgments
This work was funded by the ERC Starting Grant *UltimateRB* No. 804283. We acknowledge the access to several computational resources, all of which were used for this work: PRACE for awarding us access to MareNostrum4 at the Barcelona Supercomputing Center (BSC), Spain and IRENE at Très Grand Centre de Calcul (TGCC) du CEA, France (project 2021250115), and EuroHPC for awarding us access to Discoverer at Sofiatech, Bulgaria (No. EHPC-REG-2022R03-208).

References

Aguirre Guzmán, A. J., Madonia, M., Cheng, J. S., Ostilla-Mónico, R., Clercx, H. J., & Kunnen, R. P. (2020). Competition between Ekman plumes and vortex condensates in rapidly rotating thermal convection. *Physical Review Letters*, *125*(21), 214501. https://doi.org/10.1103/physrevlett.125.214501

Ahlers, G., Grossmann, S., & Lohse, D. (2009). Heat transfer and large scale dynamics in turbulent Rayleigh-Bénard convection. *Reviews of Modern Physics*, *81*(2), 503–537. https://doi.org/10.1103/revmodphys.81.503

Al-Shamali, F., Heimpel, M., & Aurnou, J. (2004). Varying the spherical shell geometry in rotating thermal convection. *Geophysical & Astrophysical Fluid Dynamics*, *98*(2), 153–169. https://doi.org/10.1080/03091920410001659281

Amit, H., Choblet, G., Tobie, G., Terra-Nova, F., Čadek, O., & Bouffard, M. (2020). Cooling patterns in rotating thin spherical shells—Application to Titan's subsurface ocean. *ICARUS*, *338*, 113509. https://doi.org/10.1016/j.icarus.2019.113509

Ashkenazy, Y., & Tziperman, E. (2021). Dynamic Europa Ocean shows transient Taylor columns and convection driven by ice melting and salinity. *Nature Communications*, *12*(1), 6376. https://doi.org/10.1038/s41467-021-26710-0

Aurnou, J., Calkins, M., Cheng, J., Julien, K., King, E., Nieves, D., et al. (2015). Rotating convective turbulence in Earth and planetary cores. *Physics of the Earth and Planetary Interiors*, *246*, 52–71. https://doi.org/10.1016/j.pepi.2015.07.001

Barik, A., Triana, S. A., Calkins, M., Stanley, S., & Aurnou, J. (2023). Onset of convection in rotating spherical shells: Variations with radius ratio. *Earth and Space Science*, *10*(1), e2022EA002606. https://doi.org/10.1029/2022ea002606

Beuthe, M., Rivoldini, A., & Trinh, A. (2016). Enceladus's and Dione's floating ice shells supported by minimum stress isostasy. *Geophysical Research Letters*, *43*(19), 10088–10096. https://doi.org/10.1002/2016gl070650

Bire, S., Kang, W., Ramadhan, A., Campin, J.-M., & Marshall, J. (2022). Exploring Ocean circulation on icy moons heated from below. *Journal of Geophysical Research: Planets*, *127*(3), e2021JE007025. https://doi.org/10.1029/2021je007025

Busse, F. H. (1970). Thermal instabilities in rapidly rotating systems. *Journal of Fluid Mechanics*, *44*(3), 441–460. https://doi.org/10.1017/s0022112070001921

Busse, F. H. (1983). A model of mean zonal flows in the major planets. *Geophysical & Astrophysical Fluid Dynamics*, *23*(2), 153–174. https://doi.org/10.1080/03091928308221746

Čadek, O., Souček, O., Běhounková, M., Choblet, G., Tobie, G., & Hron, J. (2019). Long-term stability of Enceladus' uneven ice shell. *ICARUS*, *319*, 476–484. https://doi.org/10.1016/j.icarus.2018.10.003

Chandrasekhar, S. (1961). *Hydrodynamic and hydromagnetic stability*. Oxford University Press.

Cheng, J. S., Stellmach, S., Ribeiro, A., Grannan, A., King, E. M., & Aurnou, J. M. (2015). Laboratory-numerical models of rapidly rotating convection in planetary cores. *Geophysical Journal International*, *201*, 1–17. https://doi.org/10.1093/gji/ggu480

Chyba, C. F., & Hand, K. P. (2005). Astrobiology: The study of the living universe. *Annual Review of Astronomy and Astrophysics*, *43*(1), 31–74. https://doi.org/10.1146/annurev.astro.43.051804.102202

Dormy, E., Soward, A. M., Jones, C. A., Jault, D., & Cardin, P. (2004). The onset of thermal convection in rotating spherical shells. *Journal of Fluid Mechanics*, *501*, 43–70. https://doi.org/10.1017/s0022112003007316

Ecke, R. E., & Niemela, J. J. (2014). Heat transport in the geostrophic regime of rotating Rayleigh-Bénard convection. *Physical Review Letters*, *113*(11), 114301. https://doi.org/10.1103/physrevlett.113.114301
Ecke, R. E., & Shishkina, O. (2023). Turbulent rotating Rayleigh-Bénard convection. *Annual Review of Fluid Mechanics*, *55*(1), 603–638. https://doi.org/10.1146/annurev-fluid-120720-020446
Gastine, T., & Aurnou, J. M. (2023). Latitudinal regionalization of rotating spherical shell convection. *Journal of Fluid Mechanics*, *954*, R1. https://doi.org/10.1017/jfm.2022.1010
Gastine, T., Wicht, J., & Aubert, J. (2016). Scaling regimes in spherical shell rotating convection. *Journal of Fluid Mechanics*, *808*, 690–732. https://doi.org/10.1017/jfm.2016.659
Gastine, T., Wicht, J., & Aurnou, J. M. (2015). Turbulent Rayleigh–Bénard convection in spherical shells. *Journal of Fluid Mechanics*, *778*, 721–764. https://doi.org/10.1017/jfm.2015.401
Hartmann, R. (2023). Data support for "Toward understanding polar heat transport enhancement in subglacial oceans on icy moons" [Dataset]. 4TU.ResearchData. https://doi.org/10.4121/f1fd2e8c-8c1e-43da-bada-8e73aae4c587
Hartmann, R., Yerragolam, G. S., Verzicco, R., Lohse, D., & Stevens, R. J. A. M. (2023). Optimal heat transport in rotating Rayleigh-Bénard convection at large Rayleigh numbers. *Physical Review Fluids*, *8*, 083501. https://doi.org/10.1103/physrevfluids.8.083501
Hemingway, D. J., & Mittal, T. (2019). Enceladus's ice shell structure as a window on internal heat production. *ICARUS*, *332*, 111–131. https://doi.org/10.1016/j.icarus.2019.03.011
Julien, K., Aurnou, J. M., Calkins, M. A., Knobloch, E., Marti, P., Stellmach, S., & Vasil, G. M. (2016). A nonlinear model for rotationally constrained convection with Ekman pumping. *Journal of Fluid Mechanics*, *798*, 50–87. https://doi.org/10.1017/jfm.2016.225
Julien, K., Knobloch, E., Rubio, A. M., & Vasil, G. M. (2012). Heat transport in low-Rossby-number Rayleigh-Bénard convection. *Physical Review Letters*, *109*(25), 254503. https://doi.org/10.1103/physrevlett.109.254503
Julien, K., Legg, S., McWilliams, J., & Werne, J. (1996). Rapidly rotating Rayleigh-Bénard convection. *Journal of Fluid Mechanics*, *322*, 243–273. https://doi.org/10.1017/s0022112096002789
Julien, K., Rubio, A., Grooms, I., & Knobloch, E. (2012). Statistical and physical balances in low Rossby number Rayleigh-Bénard convection. *Geophysical & Astrophysical Fluid Dynamics*, *106*(4–5), 392–428. https://doi.org/10.1080/03091929.2012.696109
Kang, W. (2022). Different ice-shell geometries on Europa and Enceladus due to their different sizes: Impacts of ocean heat transport. *The Astrophysical Journal*, *934*(2), 116. https://doi.org/10.3847/1538-4357/ac779c
Kang, W., & Jansen, M. (2022). On icy ocean worlds, size controls ice shell geometry. *The Astrophysical Journal*, *935*(2), 103. https://doi.org/10.3847/1538-4357/ac7a32
Kang, W., Mittal, T., Bire, S., Campin, J.-M., & Marshall, J. (2022). How does salinity shape ocean circulation and ice geometry on Enceladus and other icy satellites? *Science Advances*, *8*(29), eabm4665. https://doi.org/10.1126/sciadv.abm4665
Kihoulou, M., Čadek, O., Kvorka, J., Kalousová, K., Choblet, G., & Tobie, G. (2023). Topographic response to ocean heat flux anomaly on the icy moons of Jupiter and Saturn. *ICARUS*, *391*, 115337. https://doi.org/10.1016/j.icarus.2022.115337
King, E. M., & Aurnou, J. M. (2013). Turbulent convection in liquid metal with and without rotation. *Proceedings of the National Academy of Sciences of the United States of America*, *110*(17), 6688–6693. https://doi.org/10.1073/pnas.1217553110
King, E. M., Stellmach, S., & Aurnou, J. M. (2012). Heat transfer by rapidly rotating Rayleigh-Bénard convection. *Journal of Fluid Mechanics*, *691*, 568–582. https://doi.org/10.1017/jfm.2011.493
King, E. M., Stellmach, S., & Buffett, B. (2013). Scaling behaviour in Rayleigh-Bénard convection with and without rotation. *Journal of Fluid Mechanics*, *717*, 449–471. https://doi.org/10.1017/jfm.2012.586
Kunnen, R. P. J. (2021). The geostrophic regime of rapidly rotating turbulent convection. *Journal of Turbulence*, *22*(4–5), 267–296. https://doi.org/10.1080/14685248.2021.1876877
Kunnen, R. P. J., Clercx, H. J. H., & Geurts, B. J. (2006). Heat flux intensification by vortical flow localization in rotating convection. *Physical Review E*, *74*(5), 056306. https://doi.org/10.1103/physreve.74.056306
Kunnen, R. P. J., Stevens, R. J. A. M., Overkamp, J., Sun, C., Heijst, G. J. F. v., & Clercx, H. J. H. (2011). The role of Stewartson and Ekman layers in turbulent rotating Rayleigh-Bénard convection. *Journal of Fluid Mechanics*, *688*, 422–442. https://doi.org/10.1017/jfm.2011.383
Kvorka, J., & Čadek, O. (2022). A numerical model of convective heat transfer in Titan's subsurface ocean. *Icarus*, *376*, 114853. https://doi.org/10.1016/j.icarus.2021.114853
Nimmo, F., & Pappalardo, R. T. (2016). Ocean worlds in the outer solar system. *Journal of Geophysical Research: Planets*, *121*(8), 1378–1399. https://doi.org/10.1002/2016je005081
Plumley, M., & Julien, K. (2019). Scaling laws in Rayleigh-Bénard convection. *Earth and Space Science*, *6*(9), 1580–1592. https://doi.org/10.1029/2019ea000583
Plumley, M., Julien, K., Marti, P., & Stellmach, S. (2016). The effects of Ekman pumping on quasi-geostrophic Rayleigh-Bénard convection. *Journal of Fluid Mechanics*, *803*, 51–71. https://doi.org/10.1017/jfm.2016.452
Proudman, J. (1916). On the motion of solids in a liquid possessing vorticity. *Proceedings of the Royal Society of London, Series A: Mathematical and Physical Sciences*, *92*, 408–424.
Roberts, P. H. (1968). On the thermal instability of a rotating-fluid sphere containing heat sources. *Philosophical Transactions of the Royal Society of London Series A*, *263*(1136), 93–117.
Rossby, H. T. (1969). A study of Bénard convection with and without rotation. *Journal of Fluid Mechanics*, *36*(2), 309–335. https://doi.org/10.1017/s0022112069001674
Santelli, L., Orlandi, P., & Verzicco, R. (2020). A finite-difference scheme for three-dimensional incompressible flows in spherical coordinates. *Journal of Computational Physics*, *424*, 109848. https://doi.org/10.1016/j.jcp.2020.109848
Shishkina, O., Stevens, R. J. A. M., Grossmann, S., & Lohse, D. (2010). Boundary layer structure in turbulent thermal convection and its consequences for the required numerical resolution. *New Journal of Physics*, *12*(7), 075022. https://doi.org/10.1088/1367-2630/12/7/075022
Soderlund, K. M. (2019). Ocean dynamics of outer solar system satellites. *Geophysical Research Letters*, *46*(15), 8700–8710. https://doi.org/10.1029/2018gl081880
Soderlund, K. M., King, E. M., & Aurnou, J. M. (2012). The influence of magnetic fields in planetary dynamo models. *Earth and Planetary Science Letters*, *333–334*, 9–20. https://doi.org/10.1016/j.epsl.2012.03.038
Sprague, M., Julien, K., Knobloch, E., & Werne, J. (2006). Numerical simulation of an asymptotically reduced system for rotationally constrained convection. *Journal of Fluid Mechanics*, *551*(-1), 141–174. https://doi.org/10.1017/s0022112005008499
Stellmach, S., Lischper, M., Julien, K., Vasil, G., Cheng, J. S., Ribeiro, A., et al. (2014). Approaching the asymptotic regime of rapidly rotating convection: Boundary layers versus interior dynamics. *Physical Review Letters*, *113*(25), 254501. https://doi.org/10.1103/physrevlett.113.254501

Stevens, R. J. A. M., Blass, A., Zhu, X., Verzicco, R., & Lohse, D. (2018). Turbulent thermal superstructures in Rayleigh-Bénard convection. *Physical Review Fluids*, *3*(4), 041501(R). https://doi.org/10.1103/physrevfluids.3.041501

Stevens, R. J. A. M., Clercx, H. J. H., & Lohse, D. (2010). Optimal Prandtl number for heat transfer in rotating Rayleigh-Bénard convection. *New Journal of Physics*, *12*(7), 075005. https://doi.org/10.1088/1367-2630/12/7/075005

Stevens, R. J. A. M., Clercx, H. J. H., & Lohse, D. (2013). Heat transport and flow structure in rotating Rayleigh-Bénard convection. *European Journal of Mechanics B: Fluids*, *40*, 41–49. https://doi.org/10.1016/j.euromechflu.2013.01.004

Stevens, R. J. A. M., Zhong, J.-Q., Clercx, H. J. H., Ahlers, G., & Lohse, D. (2009). Transitions between turbulent states in rotating Rayleigh-Bénard convection. *Physical Review Letters*, *103*(2), 024503. https://doi.org/10.1103/physrevlett.103.024503

Taylor, G. I. (1917). Motion of solids in fluids when the flow is not irrotational. *Proceedings of the Royal Society of London, Series A: Mathematical and Physical Sciences*, *93*(648), 99–113.

Taylor, G. I. (1923). Stability of a viscous liquid contained between two rotating cylinders. *Philosophical Transactions of the Royal Society of London Series A*, *223*, 289–343.

van der Poel, E. P., Stevens, R. J. A. M., & Lohse, D. (2013). Comparison between two and three dimensional Rayleigh-Bénard convection. *Journal of Fluid Mechanics*, *736*, 177–194. https://doi.org/10.1017/jfm.2013.488

Vance, S. D., Panning, M. P., Stähler, S., Cammarano, F., Bills, B. G., Tobie, G., et al. (2018). Geophysical investigations of habitability in ice-covered ocean worlds. *Journal of Geophysical Research: Planets*, *123*(1), 180–205. https://doi.org/10.1002/2017je005341

Wang, G., Santelli, L., Lohse, D., Verzicco, R., & Stevens, R. J. A. M. (2021). Diffusion-free scaling in rotating spherical Rayleigh-Bénard convection. *Geophysical Research Letters*, *48*(20), e2021GL095017. https://doi.org/10.1029/2021gl095017

Wang, G., Santelli, L., Verzicco, R., Lohse, D., & Stevens, R. J. A. M. (2022). Off-centre gravity induces large-scale flow patterns in spherical Rayleigh–Bénard convection. *Journal of Fluid Mechanics*, *942*, A21. https://doi.org/10.1017/jfm.2022.360

Weiss, S., Stevens, R. J. A. M., Zhong, J.-Q., Clercx, H. J. H., Lohse, D., & Ahlers, G. (2010). Finite-size effects lead to supercritical bifurcations in turbulent rotating Rayleigh-Bénard convection. *Physical Review Letters*, *105*(22), 224501. https://doi.org/10.1103/physrevlett.105.224501

Weiss, S., Wei, P., & Ahlers, G. (2016). Heat-transport enhancement in rotating turbulent Rayleigh-Bénard convection. *Physical Review E*, *93*(4), 043102. https://doi.org/10.1103/physreve.93.043102

Yang, Y., Verzicco, R., Lohse, D., & Stevens, R. J. A. M. (2020). What rotation rate maximizes heat transport in rotating Rayleigh-Bénard convection with Prandtl number larger than one? *Physical Review Fluids*, *5*(5), 053501. https://doi.org/10.1103/physrevfluids.5.053501

Zeng, Y., & Jansen, M. F. (2021). Ocean circulation on Enceladus with a high-versus low-salinity ocean. *Planetary Science Journal*, *2*(4), 151. https://doi.org/10.3847/psj/ac1114

Zhong, J.-Q., Stevens, R. J. A. M., Clercx, H. J. H., Verzicco, R., Lohse, D., & Ahlers, G. (2009). Prandtl-Rayleigh-and Rossby-number dependence of heat transport in turbulent rotating Rayleigh-Bénard convection. *Physical Review Letters*, *102*(4), 044502. https://doi.org/10.1103/physrevlett.102.044502

References From the Supporting Information

Kunnen, R. P. J., Ostilla-Mónico, R., Poel, E. P. V. D., Verzicco, R., & Lohse, D. (2016). Transition to geostrophic convection: The role of the boundary conditions. *Journal of Fluid Mechanics*, *799*, 413–432. https://doi.org/10.1017/jfm.2016.394